ACS APPLIED MATERIALS & INTERFACES

Research Article

www.acsami.org

Delayed Fluorescence in a Solution-Processable Pure Red Molecular Organic Emitter Based on Dithienylbenzothiadiazole: A Joint Optical, Electroluminescence, and Magnetoelectroluminescence Study

Ping Chen,[†,§] Li-Ping Wang,[‡] Wan-Yi Tan,[‡] Qi-Ming Peng,[†] Shi-Tong Zhang,[†] Xu-Hui Zhu,*[,‡] and Feng Li*[,†]

[†]State Key Laboratory of Supramolecular Structure and Materials, Jilin University, Changchun, 130012, China

[‡]Institute of Polymer Optoelectronic Materials and Devices, State Key Laboratory of Luminescent Materials and Devices, South China University of Technology, Guangzhou 510640, China

[§]School of Physical Science and Technology, MOE Key Laboratory on Luminescence and Real-Time Analysis, Southwest University, Chongqing 400715, P. R. China

Supporting Information

ABSTRACT: The discovery of triplet excitons participating in the photoluminescent processes in a growing number of pure organic emitters represents an exciting impetus for a diversity of promising opto, bio, and optoelectronic applications. In this contribution, we have studied a small-molecule dithienylbenzothiadiazole-based red-emitting dye **red-1b**, which shows clearly delayed fluorescence under optical and electrical excitation. The OLED device that contained **red-1b** as a *nondoped* solution-processable emitter exhibited a moderately high utilization of exciton amounting to ≈31% and slow efficiency roll-off. Magnetoelectroluminescence measurements revealed the coexistence of reverse intersystem crossing from the lowest triplet state to singlet state (RISC, E-type triplet to singlet up-conversion) and triplet−triplet annihilation (TTA, P-type triplet to singlet up-conversion). Specifically, in low current-density regime, the moderately high exciton utilization is attributed to RISC (i.e., thermally activated delayed fluorescence, TADF), whereas in high current-density regime, TTA may contribute to suppressing efficiency roll-off. Furthermore, the results showed that **red-1b** may represent a new kind of organic red emitters that display delayed fluorescence in a way differing from the few red emitters investigated so far.

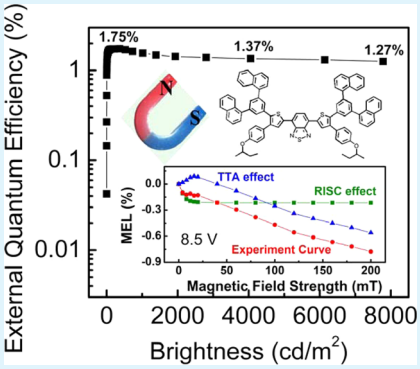

KEYWORDS: *exciton utilization, reverse intersystem crossing, triplet−triplet annihilation, electroluminescence, magnetoelectroluminescence*

1. INTRODUCTION

Organic fluorophores exhibiting delayed fluorescence have gained very recently a growing momentum in organic light-emitting diodes (OLEDs),[1−5] electrogenerated chemiluminescence,[6] and time-resolved fluorescence imaging.[7] Consequently, they may eventually provide a low-cost alternative to phosphorescent complexes that contain expensive and scarce metals, in particular for high-performance OLED displays and solid-state lighting.

Delayed fluorescence can stem from three different processes: (i) reverse intersystem crossing (RISC) from the lowest triplet to singlet excited state (E-type T → S up-conversion, or thermally activated delay fluorescence);[8] (ii) triplet−triplet annihilation (TTA, P-type T → S up-conversion),[9] and (iii) geminate electron−hole recombination.[10] Nevertheless, in RISC, it has been shown by theoretical calculation that a higher triplet excited state may potentially be involved, leading to the so-called "hot exciton" mechanism, provided that the energy barrier between $T_1 \rightarrow S_1$ is sufficiently high.[4,5]

Owing to the enormous prospects, a considerable number of organic emitters displaying E-type and/or P-type delayed fluorescence have been reported, revealing rich chemical structure−property relationships.[1,11−15] Remarkably, Adachi et al. disclosed high-efficiency OLEDs by utilizing thermally activated delay fluorescence materials (TADF, E-type) that were previously achievable only by phosphorescent metal complexes, amounting to a near unity of internal quantum efficiency.[16]

In light of these advances, we report herein delayed fluorescence in a pure red molecular emitter based on dithienylbenzothiadiazole, denoted as **red-1b**.[17] A combined optical, electroluminescence (EL), and magnetoelectrolumines-

Received: December 8, 2014
Accepted: January 13, 2015
Published: January 13, 2015

DOI: 10.1021/am508574m
ACS Appl. Mater. Interfaces 2015, 7, 2972−2978

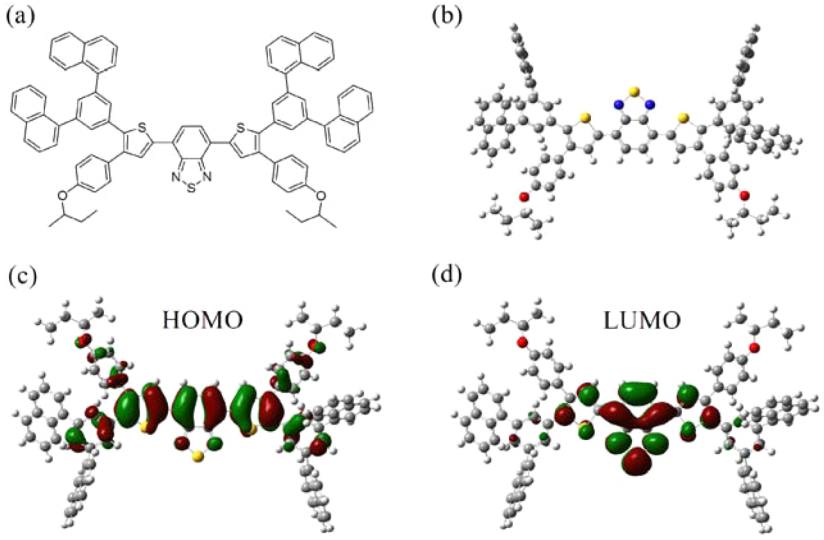

Figure 1. (a) The molecular structure of **red-1b**. (b) The optimized configuration of **red-1b**. (c) HOMO and (d) LUMO of **red-1b**, calculated by Gaussian 09 with density function theory (DFT) of B3LYP/6-31(d,p).

cence study reveals that both the thermally activated reverse intersystem crossing (E-type) and triplet−triplet annihilation (P-type) processes contribute to the resulting EL performance, thus yielding a moderately high utilization of the exciton and a small roll-off of EL efficiency in the nondoped solution-processed emitting layer. Furthermore, the results showed that **red-1b** undergoes a different route in acquiring delayed fluorescence from only a few other red emitters described thus far.

2. EXPERIMENTAL SECTION

2.1. OLED Fabrication. Patterned indium−tin oxide (ITO, 15 Ω/square)-coated glass substrates were cleaned successively with ethanol, acetone, and detergent water in an ultrasonic bath. After treatment with oxygen plasma, PEDOT:PSS was spin-coated onto the ITO substrate (3500 rpm/min, 35 nm) and then dried at 120 °C for 30 min. Then, 25 nm PVK film was coated on top of the PEDOT:PSS layer from a 10 mg/mL chloroform solution at a speed of 3000 rpm, and dried at 100 °C for 15 min. Subsequently, a 30 nm thin film of **red-1b** was spin-coated from a 20 mg/mL *p*-xylene solution at a speed of 2500 rpm, and dried at 120 °C for 15 min. The organic electron-transport layer TPBi as well as the CsF/Al cathode were deposited by thermal evaporation under a pressure of <5 × 10^{-4} Pa. The active area was 2 × 2 mm^2.

2.2. OLED and Magnetoelectroluminescence Measurements. Immediately after device preparation, the tests of *I*−*V* characteristics were carried out by the Keithley 2400 SourceMeter. Brightness was synchronously obtained by PR650 SpectraColorimeter. During MEL measurement, the device was mounted between two pole pieces of an electromagnet. The magnetic field with maximum strength of ±300 mT was applied parallel to the device surface and perpendicular to the current direction. The Keithley 2612 Dual-Channels SourceMeter was used to provide the voltage bias from one channel and simultaneously recorded the current signals. The other channel of Keithley 2612 was used to record the EL intensity collected by the photomultiplier. The photomultiplier was placed far away from the electromagnet to make sure there is no magnetic field dependence on its output. All the measurements were carried out at room temperature under ambient conditions.

3. RESULTS AND DISCUSSION

3.1. Molecular Modeling and Optical Properties. **Red-1b** represents a D-A-D type chemical structure, consisting of a (3,5-di(1-naphthyl)phenyl)thienyl group as an electron donor (D) and benzothiadiazole as an electron acceptor (A) (Figure 1a).[17] The optimized spatial configuration is shown in Figure 1b, by Gaussian 09 based on Density Functional Theory (DFT) with the method of B3LYP/6-31(d,p).

The theoretical calculation suggests that the thiophene planes are nearly coplanar with the benzothiodiazole plane, showing a dihedral angle of ≈8° in **red-1b**, respectively. Further, the doubly naphthylated "phenyl" ring is twisted against the neighboring thienyl ring by a dihedral angle of ≈44°. The HOMO is mainly concentrated on both thienyl and benzothiadiazole moieties, while the LUMO is merely localized on benzothiadiazole moieties. Therefore, there seems certain overlap between the HOMO and LUMO.

The charge transfer character of the excited state of **red-1b** was evidenced by the red shift of solution emission maximum (λ_{em}) upon increasing solvent polarity. For instance, λ_{em} shifts from 593 to 609 nm when replacing toluene by dichloromethane. For the solid film of **red-1b** spin-casted from a toluene solution, a red emission with λ_{em} ≈622 nm and an unresolved shoulder at ca. 660 nm was observed.[17] The molecular interaction should cause the red shift compared to the emission of solution.

To identify the contribution of delayed fluorescence, transient PL decay of **red-1b** spin-cast thin film was measured (Figure 2a). As can be seen, the transient PL decay of **red-1b** exhibits a clear delayed fluorescence component, from which we can figure out the delayed fluorescence lifetime of **red-1b** is about 828 ns. Based on the prompt solid-state photoluminescent (PL) spectrum in ambient air and the 2 μs delayed PL spectrum at 77 K in toluene solution (the higher energy part and the lower energy part are referred to as delayed fluorescence and phosphorescence, respectively), we can determine roughly the energies of lowest singlet (S_1) and triplet (T_1) states, by deriving respectively from the corresponding onset of the emission bands (Figure 2b).[10,18] The $\Delta E_{S\text{-}T}$ of **red-1b** is estimated to be ∼0.40 eV.

DOI: 10.1021/am508574m
ACS Appl. Mater. Interfaces 2015, 7, 2972−2978

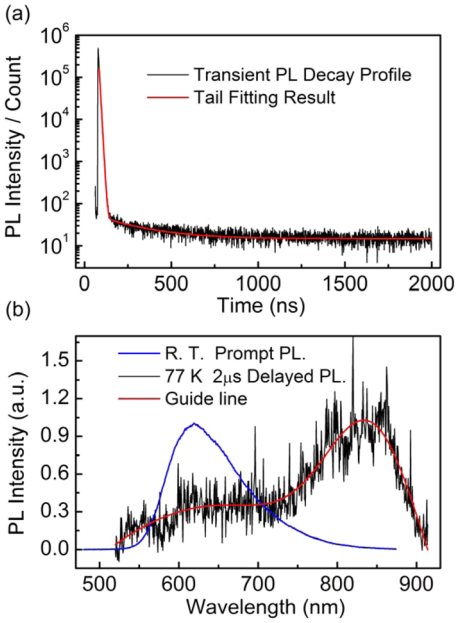

Figure 2. (a) Transient PL decay profile for **red-1b** spin-cast thin film at room temperature. The red solid line is fitting the tail to estimate the lifetime of the delayed component of 828 ns. (b) PL spectra of **red-1b** in 10^{-5} M toluene solution (excitation wavelength of 410 nm): prompt component at room temperature, and 2 μs delayed component at 77 K (phosphorescence).

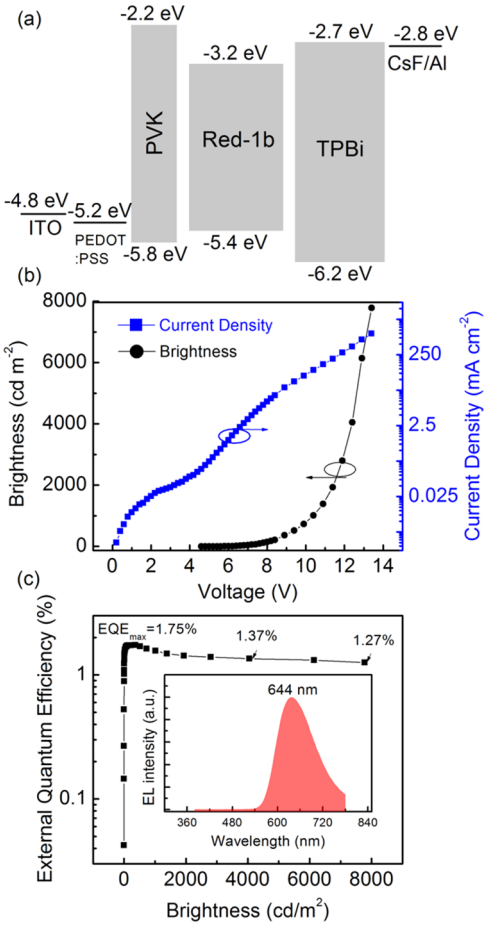

Figure 3. OLED performance of **red-1b**: (a) device structure and energy-level diagrams; (b) brightness–current density–voltage (B–I–V) characteristics; and (c) external quantum efficiency (EQE) versus brightness. The inset shows the EL spectra.

3.2. OLED Characteristics. To facilitate device characterization, **red-1b** was investigated as a nondoped solution-processed emitter in an OLED structure (ITO/PEDOT:PSS/PVK/**red-1b**/TPBi/CsF/Al, Figure 3a) that differed from the previous report.[17] PEDOT:PSS = poly(3,4-ethylene dioxythiophene):poly(styrenesulfonate), PVK = poly(9-vinylcarbazole), TPBi = 1,3,5-tris(*N*-phenylbenzimidizol-2-yl)-benzene. PVK and TPBI functioned as electron-blocking and electron-transporting material, respectively.

The device showed multiple prominent characteristics. It gave a pure red emission with a maximum spectral peak around 644 nm with CIE coordinates (0.65, 0.33) (Figure 3c). The EL spectra remained stable with increasing the bias from 5 to 12 V (Figure S1, Supporting Information). A high brightness of ~7800 cd m^{-2} was obtained (Figure 3c). Furthermore, the device efficiency displayed a slow roll-off. For instance, the maximum external quantum efficiency (EQE) of 1.75% (corresponding to a luminous efficiency of 1.22 cd/A) at a luminance of 177 cd m^{-2} decreased to 1.27% even at the maximal luminance 7782 cd m^{-2} (Figure 3c).

Through the relationship of

$$\eta_{ext} = \eta_s \phi_{fl} n \gamma \quad (1)$$

where η_s is the fraction of singlet exciton, ϕ_{fl} the PL efficiency of **red-1b** thin film, n the optical out-coupling, and γ the charge-balance factor, the ϕ_{fl} was determined to be 28% from 30 nm **red-1b** thin film cast on quartz under ambient condition when excited at a wavelength of 330 nm in integrating sphere (fluoroSENS-9000), and we roughly assumed $n \approx 20\%$ and $\gamma \approx 100\%$ for simplicity. Thus, the η_s was estimated to be 31.3%, *overcoming the 25% theoretical limit imposed by spin statistics.*

3.3. EL Transient Decay. To identify whether the triplet exciton of the emitter **red-1b** contributed to its electroluminescence, we measured the transient EL decay. A rectangular pulse voltage (6 V, corresponding to 12 mA cm^{-2} steady state current density) was applied to the OLED device with a repetition rate of 1 kHz and pulse width of 50 μs. The EL signal was collected by an optical fiber connected to Hamamatsu photomultiplier (H5738-01) with a resolution of 0.78 ns.[19,20]

As shown in Figure 4, when no offset bias was applied in mode (i) the curves show substantial delayed EL components, indicating a considerable contribution of delayed EL in total emission. Similar to delayed fluorescence under photoexcitation, delayed electrofluorescence can arise from RISC, TTA, and recombination of mobile and trapped charge carriers remaining in the device.[2,21,22]

In principle, RISC and TTA should not be significantly affected by the electric field strength because of the electroneutrality of excitons. By contrast, the applied bias can produce a strong effect on delayed charge recombination because the diffusion of charge carriers is directly affected by the electric field.[21,22] For instance, mobile carriers would drift away much faster from the recombination zone at a negative offset bias than the condition at a 0 V offset bias. It should be mentioned that, a negative offset bias near −10 V might be strong enough to eliminate the delayed charge recombination,[21] above which could cause damage to the device.

When mode (ii) of −10 V offset bias was applied, the delayed EL component shows an overshoot and then a substantial

DOI: 10.1021/am508574m
ACS Appl. Mater. Interfaces 2015, 7, 2972–2978

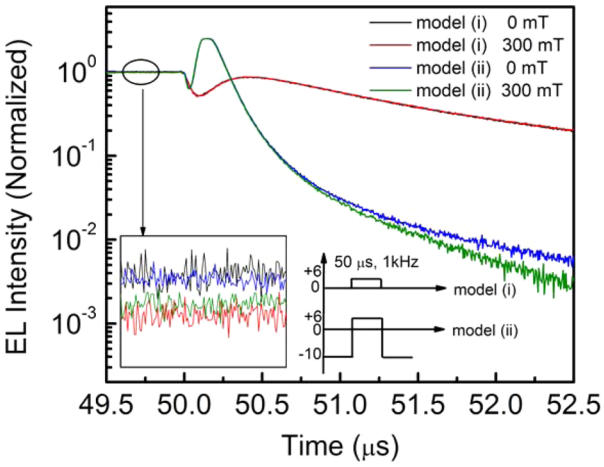

Figure 4. Transient EL decay of the **red-1b** OLED with and without magnetic field. Reverse bias of 0 and 10 V were applied in mode (i) and mode (ii), respectively.

decrease, resulting from the suppression of the delayed charge recombination. However, a long EL decay is still observed indicating that RISC or TTA is operative.

Time-resolved optical measurements have been employed as a direct method to confirm the existence of TADF and TTA. Recently we proposed another feasible method of magneto-electroluminescence (MEL), i.e., the relative variation of EL intensity versus the strength of external magnetic field, as an effective tool to study the RISC and TTA processes.[23] Since RISC and TTA are highly spin-dependent processes, they can generate sizable magnetic field responses, i.e., applying an external magnetic field can largely suppress the strength of RISC and TTA, thus diminishing the delayed EL.[23−25] Moreover, magnetic fields in low-field (≲40 mT) and high-field (≳40 mT) regimes play different roles in RISC and TTA, respectively, exhibiting different MEL responses of RISC and TTA. As a result, the MEL gains advantages over traditional time-resolved spectra: In principle, both RISC and TTA are processes in long-time scale (usually microsecond), thus it is not an easy task to discern the RISC and TTA merely from time-resolved spectra because of their complicated but similar delayed fluorescence (DF) behaviors. So, the transient EL under magnetic field was measured. As expected, the transient EL under magnetic field decayed faster at a turning point from the one without magnetic field, when mode (ii) of −10 V offset bias was applied, confirming the existence of RISC or TTA.

3.4. Magnetoelectroluminescence (MEL). The MEL is quantificationally defined as

$$\mathrm{MEL} = \Delta\mathrm{EL}/\mathrm{EL} = [\mathrm{EL}(B) - \mathrm{EL}(0)]/\mathrm{EL}(0) \quad (2)$$

where $\mathrm{EL}(B)$ and $\mathrm{EL}(0)$ represent the EL intensities with and without the applied magnetic field B, respectively.[19,20,23−35]

As discussed above, the EL of **red-1b** includes prompt fluorescence and delayed fluorescence. The prompt fluorescence comes from the direct radiative decay of singlets, while the delayed fluorescence results from RISC and TTA. Principally, the prompt fluorescence is magnetic field independent because the direct radiative decay of singlets is not affected by magnetic field. In contrast, RISC and TTA are highly magnetic field dependent processes, so only delayed fluorescence needed to be considered in MEL. The modulation of applied magnetic field on RISC can be understood as follows: In the absence of a magnetic field, the singlet and triplet CT species nearly degenerate, and thus RISC is very

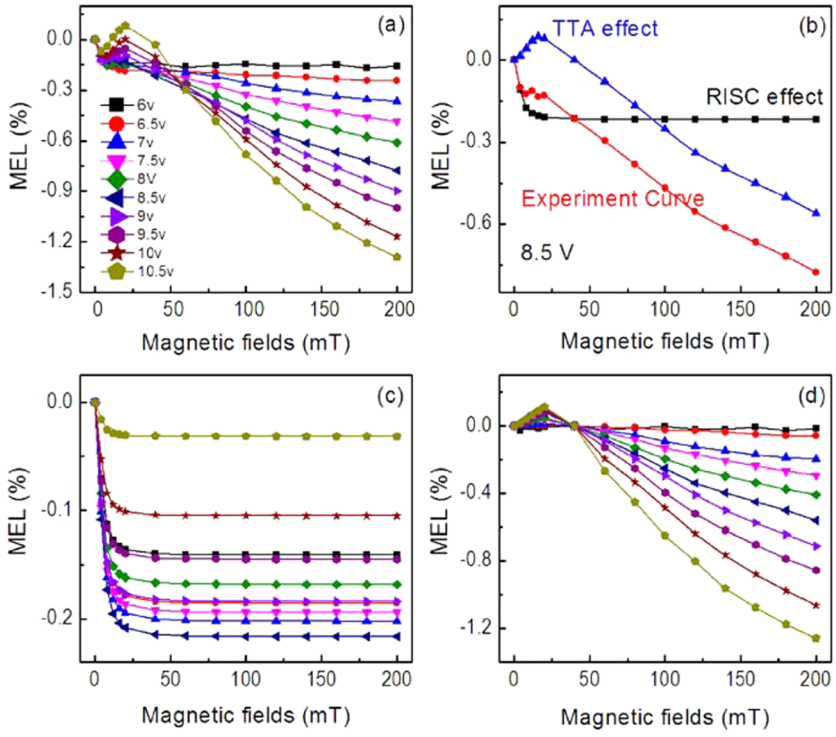

Figure 5. (a) Magnetoelectroluminescence (MEL) response of **red-1b** device under different applied bias from 6 to 10.5 V. (b) The decomposition of the MEL experimental curve into a RISC effect and TTA effect. (c) The decomposed RISC-mediated MEL. (d) TTA-mediated MEL under different applied bias. Panels c and d share the same applied bias labels denoted in panel a.

DOI: 10.1021/am508574m
ACS Appl. Mater. Interfaces 2015, 7, 2972−2978

efficient assisted by internal hyperfine field from three triplet substates (T_{-1}, T_0, and T_{+1}) to the singlet state (S).[29−31] When a higher external magnetic field than the hyperfine field is applied, the Zeeman splitting of triplet states removes the degeneracy between T_{-1}, T_{+1}, and S states, leaving only one channel for RISC from T_0 to S states. As a result, RISC is partly blocked by the magnetic field, leading to a deceased TADF.[23,24] The MEL exhibits a rapid decrease within the range of several millitesla and then tends to be saturated, which can be fitted by a Lorentzian function: MEL $\propto B^2/(B^2 + B_0^2)$. Here, B_0 is the fitting parameter denoting the saturation field of organic materials, which is in the range of several millitesla.[32] On the other hand, the TTA mediated MEL can be explained by the redistribution of singlet spin character among nine possible intermediate triplet pair-states by a function of the applied magnetic field.[36]

The MEL of the **red-1b** device consists of a rapid decrease in the low-field regime (<20 mT), followed by a slower decrease in the high-field regime (>20 mT), which cannot simply accord with the characteristic of RISC or TTA (Figure 5a). Hence, a composite model is proposed.[24] By subtracting the RISC effect from our experimental curve, we therefore consider whether the TTA effect can be obtained in the present device (the specific decomposition method can be found in the Support Information).

Taking the 8.5 V case for example, seen in Figure 5b, the subtracted MEL undergoes a small increase within the field of 20 mT, but a remarkable decrease at a higher field, hence bearing a great similarity to those TTA-mediated MELs observed in anthracene crystal[36] and amorphous OLEDs.[25,34,35]

To identify the rationality of decomposition of the MEL of the **red-1b** device, the decomposed RISC and TTA mediated MEL at different voltage bias were displayed in Figure 5, panels c and d, respectively.

The absolute value of RISC-mediated MEL first increased and then monotonically decreased with increasing the voltage bias. This behavior is quite consistent with the variation of hyperfine-field assisted MEL with applied voltage bias.[23,24,30] As compared to the RISC-mediated MEL, the TTA-mediated MEL is monotonic as a function of voltage bias.

At a higher voltage, both low-field increase and high-field decrease of TTA-mediated MEL became remarkable (Figure 5d), suggesting an enhanced TTA process,[25,34,35] because the probability of the TTA process is expected to be proportional to the square of the triplet density considering its bimolecular process, and the density of triplets is directly related to the current.

Finally, the voltage dependence of decomposed RISC and TTA-mediated MEL verifies that E-type T → S up-conversion dominated in low current level resulting in high exciton utilization, while P-type T → S up-conversion may play an important role in high current level suppressing the efficiency roll-off.

3.5. Contribution of TTA to Efficiency Roll-Off: OLEDs Based on the Doped red-1b. We further dope **red-1b** into the 1,3-bis(9-carbazolyl)benzene (mCP) matrix with various concentrations. In this host−guest system, the excitons of **red-1b** are confined in the mCP matrix by its very large band gap of ~3.5 eV.[37] This architecture can effectively control the annihilation of the triplets upon collision.[22] As **red-1b** concentration increases from 13.7 to 100 wt %, more apparent TTA-mediated MEL can be seen (Figure 6a), suggesting an enhanced TTA process at a higher **red-1b** concentration.

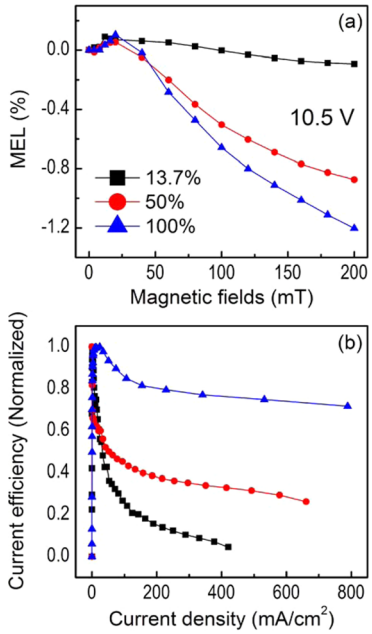

Figure 6. (a) MEL responses of **red-1b**:mCP devices at a doped concentration of 13.7, 50, and 100 wt %, under the applied bias of 10.5 V. (b) Normalized current efficiency of the **red-1b**:mCP OLED devices. The **red-1b**:mCP device had the same OLED structure presented in Figure 4 except for the emitting layer. The maximum magnetic strength is 200 mT.

Figure 6b summarizes the normalized current efficiency for the OLED devices with different **red-1b** concentrations. The lower the **red-1b** concentration, the more rapidly the device efficiency rolled off. This result indicates that the TTA indeed plays a contributing role in suppressing device efficiency roll-off.

Furthermore, it is of interest to note that the way the emitter **red-1b** acquires delayed fluorescence appears to be different from those of the few other red emitters reported so far, such as TPA-NZP ("hot exciton" mechanism),[4] DCF-MPYM (TADF),[7] DCJTB,[23] rhodamine and ATTO-532 (geminate electron−hole pair recombination).[38] On the other hand, the coexistence of TADF and TTF upconversion has been shown for some of the D-A-D type emitters that have a considerably high $\Delta E_{S\text{-}T}$.[18]

4. CONCLUSIONS

In summary, the present study has disclosed delayed fluorescence of an organic pure red emitter based on dithienylbenzothiodiazole under photo and electrical excitation. The characterization of the magnetoelectroluminesce experiments has revealed that the coexistence of E-type (TADF) and P-type (TTA) triplet to singlet up-conversion accounts for the delayed electrofluorescence. Specifically, E-type RISC (TADF) may contribute to the moderately high exciton utilization in the nondoped OLED at low operating voltages, thereby exceeding the 25% theoretical limit imposed by the spin statistics. On the other hand, the P-type TTA process may be beneficial to maintain a small efficiency roll-off at high voltages. Since **red-1b** possesses multiple attractive attributes such as simple synthesis and purification, solution processability, reversible electrochemical reduction and oxidation, and a high PL yield in solution and as films (whereas DCJTB and rhodamine and its derivatives suffer severe PL quenching in the solid state[23,38]),

DOI: 10.1021/am508574m
ACS Appl. Mater. Interfaces 2015, 7, 2972−2978

the results reported here, in particular with a clearer understanding of the delayed fluorescent properties, shall bring a renewed interest in this class of red emitters and their applications.[39−44]

■ ASSOCIATED CONTENT

Supporting Information

The EL spectra of the **red-1b OLED** at different bias from 5 V to 12 V (Figure S1) and the composition model of the experimental MEL (RISC and TTA, Figure S2). This material is available free of charge via the Internet at http://pubs.acs.org.

■ AUTHOR INFORMATION

Corresponding Authors

*E-mail: xuhuizhu@scut.edu.cn.

*E-mail: lifeng01@jlu.edu.cn.

Notes

The authors declare no competing financial interest.

■ ACKNOWLEDGMENTS

This work was financially supported by the National Natural Science Foundation (NSF) of China (Grant Nos. 61275036, 21221063, and 91233113), MOST (Grant No. 2015CB655000), and Fundamental Research Funds for the Central Universities (Grant Nos. SWU114042 and XDJK2015C046). X.H.Z. is grateful for the financial support of SCUT and NSFC (Grant Nos. 2014ZG0009, 51173051, and U1301243).

■ REFERENCES

(1) Zhang, Q.; Li, J.; Shizu, K.; Huang, S.; Hirata, S.; Miyazaki, H.; Adachi, C. Design of Efficient Thermally Activated Delayed Fluorescence Materials for Pure Blue Organic Light Emitting Diodes. *J. Am. Chem. Soc.* **2012**, *134*, 14706−14709.

(2) Uoyama, H.; Goushi, K.; Shizu, K.; Nomura, H.; Adachi, C. Highly Efficient Organic Light-Emitting Diodes From Delayed Fluorescence. *Nature* **2012**, *492*, 234−238.

(3) Li, J.; Nakagawa, T.; MacDonald, J.; Zhang, Q.; Nomura, H.; Miyazaki, H.; Adachi, C. Highly Efficient Organic Light-Emitting Diode Based on a Hidden Thermally Activated Delayed Fluorescence Channel in a Heptazine Derivative. *Adv. Mater.* **2013**, *25*, 3319−3323.

(4) Li, W.; Pan, Y.; Xiao, R.; Peng, Q.; Zhang, S.; Ma, D.; Li, F.; Sheng, F.; Wang, Y.; Yang, B.; Ma, Y. Employing ∼100% Excitons in OLEDs by Utilizing a Fluorescent Molecule with Hybridized Local and Charge-Transfer Excited State. *Adv. Funct. Mater.* **2014**, *24*, 1609−1614.

(5) Yao, L.; Zhang, S.; Wang, R.; Li, W.; Shen, F.; Yang, B.; Ma, Y. Highly Efficient Near-Infrared Organic Light-Emitting Diode Based on a Butterfly-Shaped Donor−Acceptor Chromophore with Strong Solid-State Fluorescence and a Large Proportion of Radiative Excitons. *Angew. Chem., Int. Ed.* **2014**, *53*, 2119−2123.

(6) Ishimatsu, R.; Matsunami, S.; Kasahara, T.; Mizuno, J.; Edura, T.; Adachi, C.; Nakano, K.; Imato, T. Electrogenerated Chemiluminescence of Donor−Acceptor Molecules with Thermally Activated Delayed Fluorescence. *Angew. Chem., Int. Ed.* **2014**, *53*, 6993−6996.

(7) Xiong, X.; Song, F.; Wang, J.; Zhang, Y.; Xue, Y.; Sun, L.; Jiang, N.; Gao, P.; Tian, L.; Peng, X. Thermally Activated Delayed Fluorescence of Fluorescein Derivative for Time-Resolved and Confocal Fluorescence Imaging. *J. Am. Chem. Soc.* **2014**, *136*, 9590−9597.

(8) Kaputskaya, I. A.; Ermilov, E. A.; Tannert, S.; Röder, B.; Gorbatsevich, S. K. Spectral, Kinetic and Polarization Characteristics of Luminescence of Acriflavine in Polymeric Matrix under Pulsed Excitation with Different Durations and Intensities. *Chem. Phys.* **2006**, *327*, 171−179.

(9) Nickel, B.; Roden, G. Delayed Fluorescence from the Lowest 1B +3u State of Anthracene, Due to Hetero-Triplet-Triplet Annihilation of 3anthracene* and 3xanthone*. *Chem. Phys.* **1982**, *66*, 365−376.

(10) Ewald, M.; Durocher, G. Photoionization and Recombination Delayed Fluorescence in Anthracene Single Crystals. *Chem. Phys. Lett.* **1971**, *12*, 385−388.

(11) Méhes, G.; Nomura, H.; Zhang, Q.; Nakagawa, T.; Adachi, C. Enhanced Electroluminescence Efficiency in a Spiro-Acridine Derivative through Thermally Activated Delayed Fluorescence. *Angew. Chem., Int. Ed.* **2012**, *51*, 11311−11315.

(12) Lee, S. Y.; Yasuda, T.; Nomura, H.; Adachi, C. High-efficiency Organic Light-Emitting Diodes Utilizing Thermally Activated Delayed Fluorescence from Triazine-based Donor−Acceptor Hybrid Molecules. *Appl. Phys. Lett.* **2012**, *101*, 093306.

(13) Nakagawa, T.; Ku, S. Y.; Wong, K. T.; Adachi, C. Electroluminescence Based on Thermally Activated Delayed Fluorescence Generated by a Spirobifluorene Donor−Acceptor Structure. *Chem. Commun.* **2012**, *48*, 9580−9582.

(14) Nakanotani, H.; Masui, K.; Nishide, J.; Shibata, T.; Adachi, C. Promising Operational Stability of High-efficiency Organic Light-Emitting Diodes Based on Thermally Activated Delayed Fluorescence. *Sci. Rep.* **2013**, *3*, 2127.

(15) Wang, H.; Xie, L.; Peng, Q.; Meng, L.; Wang, Y.; Yi, Y.; Wang, P. Novel Thermally Activated Delayed Fluorescence Materials−Thioxanthone Derivatives and Their Applications for Highly Efficient OLEDs. *Adv. Mater.* **2014**, *26*, 5198−5204.

(16) Nakanotani, H.; Higuchi, T.; Furukawa, T.; Masui, K.; Morimoto, K.; Numata, M.; Tanaka, H.; Sagara, Y.; Yasuda, T.; Adachi, C. High-efficiency Organic Light-Emitting Diodes with Fluorescent Emitters. *Nat. Commun.* **2014**, *5*, 4016.

(17) Huang, J.; Liu, Q.; Zou, J. H.; Zhu, X. H.; Li, A. Y.; Li, J. W.; Wu, S.; Peng, J. B.; Cao, Y.; Xia, R. D.; Bradley, D. D. C.; Roncali, J. Electroluminescence and Laser Emission of Soluble Pure Red Fluorescent Molecular Glasses Based on Dithienylbenzothiadiazole. *Adv. Funct. Mater.* **2009**, *19*, 2978−2986.

(18) Dias, F. B.; Bourdakos, K. N.; Jankus, V.; Moss, K. C.; Kamtekar, K. T.; Bhalla, V.; Santos, J.; Bryce, M. R.; Monkman, A. P. Triplet Harvesting with 100% Efficiency by Way of Thermally Activated Delayed Fluorescence in Charge Transfer OLED Emitters. *Adv. Mater.* **2013**, *25*, 3707−3714.

(19) Li, F.; Xin, L.; Liu, S.; Hu, B. Direct measurement of the Magnetic Field Effects on Carrier Mobilities and Recombination in Tri-(8-hydroxyquinoline)-aluminum Based Light-Emitting Diodes. *Appl. Phys. Lett.* **2010**, *97*, 073301.

(20) Peng, Q.; Sun, J.; Li, X.; Li, M.; Li, F. Investigation of the Magnetic Field Effects on Electron Mobility in Tri-(8-hydroxyquinoline)-aluminum Based Light-Emitting Devices. *Appl. Phys. Lett.* **2011**, *99*, 033509.

(21) Kondakov, D. Y. Characterization of Triplet−Triplet Annihilation in Organic Light-Emitting Diodes Based on Anthracene Derivatives. *J. Appl. Phys.* **2007**, *102*, 114504.

(22) Luo, Y.; Aziz, H. Correlation Between Triplet−Triplet Annihilation and Electroluminescence Efficiency in Doped Fluorescent Organic Light-Emitting Devices. *Adv. Funct. Mater.* **2010**, *20*, 1285−1293.

(23) Chen, P.; Xiong, Z.; Peng, Q.; Bai, J.; Zhang, S.; Li, F. Magneto-Electroluminescence as a Tool to Discern the Origin of Delayed Fluorescence: Reverse Intersystem Crossing or Triplet−Triplet Annihilation? *Adv. Opt. Mater.* **2014**, *2*, 142−148.

(24) Peng, Q.; Li, W.; Zhang, S.; Chen, P.; Li, F.; Ma, Y. Evidence of the Reverse Intersystem Crossing in Intra-Molecular Charge-Transfer Fluorescence-Based Organic Light-Emitting Devices Through Magneto-Electroluminescence Measurements. *Adv. Opt. Mater.* **2013**, *1*, 362−366.

(25) Liu, R.; Zhang, Y.; Lei, Y.; Chen, P.; Xiong, Z. Magnetic Field Dependent Triplet-Triplet Annihilation in Alq3-based Organic Light Emitting Diodes at Different Temperatures. *J. Appl. Phys.* **2009**, *105*, 093719.

DOI: 10.1021/am508574m
ACS Appl. Mater. Interfaces 2015, 7, 2972−2978

(26) Desai, P.; Shakya, P.; Kreouzis, T.; Gillin, W. P.; Morley, N. A.; Gibbs, M. R. J. Magnetoresistance and Efficiency Measurements of Alq3-based OLEDs. *Phys. Rev. B* **2007**, *75*, 094423.
(27) Mermer, O.; Veeraraghavan, G.; Francis, T. L.; Sheng, Y.; Nguyen, T. D.; Wohlgenannt, M.; Kohler, A.; Al-Suti, M. K.; Khan, M. S. Large Magnetoresistance in Nonmagnetic π-Conjugated Semiconductor Thin Film Devices. *Phys. Rev. B* **2005**, *72*, 205202.
(28) Bloom, F. L.; Wagemans, W.; Kemerink, M.; Koopmans, B. Separating Positive and Negative Magnetoresistance in Organic Semiconductor Devices. *Phys. Rev. Lett.* **2007**, *99*, 257201.
(29) Kalinowski, J.; Szmytkowski, J. D.; Stampor, W. Magnetic Field Effects on Emission and Current in Alq3-based Electroluminescent Diodes. *Chem. Phys. Lett.* **2003**, *378*, 380−387.
(30) Kalinowski, J.; Cocchi, M.; Virgili, D.; Di Marco, P.; Fattori, V. Magnetic Field Effects on Emission and Current in Alq3-based Electroluminescent Diodes. *Chem. Phys. Lett.* **2003**, *380*, 710−715.
(31) Hu, B.; Wu, Y. Tuning Magnetoresistance Between Positive and Negative Values in Organic Semiconductors. *Nat. Mater.* **2007**, *6*, 985−991.
(32) Sheng, Y.; Nguyen, T. D.; Veeraraghavan, G.; Mermer, O.; Wohlgenannt, M.; Qiu, S.; Scherf, U. Hyperfine Interaction and Magnetoresistance in Organic Semiconductors. *Phys. Rev. B* **2006**, *74*, 045213.
(33) Bagnich, S. A.; Niedermeier, U.; Melzer, C.; Sarfert, W.; von Seggern, H. Electron-hole Pair Mechanism for the Magnetic Field Effect in Organic Light Emitting Diodes Based on Poly(paraphenylene vinylene). *J. Appl. Phys.* **2009**, *106*, 113702.
(34) Lei, Y.; Zhang, Y.; Liu, R.; Chen, P.; Song, Q.; Xiong, Z. Driving Current and Temperature Dependent Magnetic-field Modulated Electroluminescence in Alq3-based Organic Light Emitting Diode. *Org. Electron.* **2009**, *10*, 889−894.
(35) Davis, A. H.; Bussmann, K. Large Magnetic Field Effects in Organic Light Emitting Diodes Based on Tris(8-hydroxyquinoline aluminum) (Alq3)/N,N′-Di(naphthalen-1-yl)-N,N′diphenyl-benzidine (NPB) Bilayers. *J. Vac. Sci. Technol.* **2004**, *22*, 1885−1891.
(36) MerriIfield, R. E. Theory of Magnetic Field Effects on the Mutual Annihilation of Triplet Excitons. *J. Chem. Phys.* **1968**, *48*, 4318−4319.
(37) Hu, D.; Wang, C.; Liu, H.; Wang, H.; Wang, Z.; Fei, T.; Gu, X.; Ma, Y. Silane Coupling Di-carbazoles with High Triplet Energy as Host Materials for Highly Efficient Blue Phosphorescent Devices. *J. Mater. Chem.* **2009**, *19*, 6143−6148.
(38) Aydemir, M.; Jankus, V.; Dias, F. B.; Monkman, A. The Key Role of Geminate Electron−hole Pair Recombination in the Delayed Fluorescence in Rhodamine 6G and ATTO-532. *Phys. Chem. Chem. Phys.* **2014**, *16*, 21543−21549.
(39) Huang, J.; Zhu, X. H.; Li, C.; Xia, Y. J.; Peng, J. B.; Cao, Y. Amorphous Fluorescent Organic Emitters for Efficient Solution-Processed Pure Red Electroluminescence: Synthesis, Purification, Morphology, Solid-State Photoluminescence, and Device Characterizations. *J. Org. Chem.* **2007**, *72*, 8580−8583.
(40) Huang, J.; Qiao, X.; Xia, Y. J.; Zhu, X.; Ma, D.; Cao, Y.; Roncali, J. A Dithienylbenzothiadiazole Pure Red Molecular Emitter with Electron Transport and Exciton Self-Confinement for Nondoped Organic Red-Light-Emitting Diodes. *Adv. Mater.* **2008**, *20*, 4172−4175.
(41) Wang, Y. C.; Huang, J.; Zhou, H.; Ma, G.; Qian, S.; Zhu, X. Synthesis, Optical Properties and Ultrafast Dynamics of a 2,1,3-benzothiadiazole-based Red Emitter with Intense Fluorescence and Large Two-Photon Absorption Cross-Section. *Dyes Pigm.* **2012**, *92*, 573−579.
(42) Tang, S.; Tan, W.; Zhu, X.; Edman, L. Small-molecule Light-Emitting Electrochemical Cells: Evidence for *In Situ* Electrochemical Doping and Functional Operation. *Chem. Commun.* **2013**, *49*, 4926−4928.
(43) Shen, M.; Zhu, X.; Bard, A. J. Electrogenerated Chemiluminescence of Solutions, Films, and Nanoparticles of Dithienylbenzothiadiazole-Based Donor−Acceptor−Donor Red Fluorophore. Fluorescence Quenching Study of Organic Nanoparticles. *J. Am. Chem. Soc.* **2013**, *135*, 8868−8873.
(44) Shen, M.; Rodriguez Lopez, J.; Huang, J.; Liu, Q.; Zhu, X.; Bard, A. J. Electrochemistry and Electrogenerated Chemiluminescence of Dithienylbenzothiadiazole Derivative. Differential Reactivity of Donor and Acceptor Groups and Simulations of Radical Cation−Anion and Dication−Radical Anion Annihilations. *J. Am. Chem. Soc.* **2010**, *132*, 13453−13461.

DOI: 10.1021/am508574m
ACS Appl. Mater. Interfaces 2015, 7, 2972−2978